Scientia Iranica B (2020) 27(3), 1266–1276

Sharif University of Technology
Scientia Iranica
Transactions B: Mechanical Engineering
http://scientiairanica.sharif.edu

Hyperelastic modeling of sino-nasal tissue for haptic neurosurgery simulation

S. Sadeghnejad[a], N. Elyasi[a], F. Farahmand[a,*], Gh. Vossoughi[a], and S.M. Sadr Hosseini[b]

a. *Mechanical Engineering Department, Sharif University of Technology, Tehran, Iran.*
b. *Vali-e-Asr Hospital, School of Medicine, Tehran University of Medical Sciences, Tehran, Iran.*

Received 26 January 2018; received in revised form 25 November 2018; accepted 16 February 2019

KEYWORDS
Endoscopic sinus and skull base surgery;
Surgical simulation system;
Inverse finite element method;
SQP algorithm;
Hyperelastic models;
Sino-nasal tissue.

Abstract. The aim of this research is to provide a simple, yet realistic, model of the sino-nasal tissue as a major requirement for developing more efficient endoscopic neurosurgery simulation systems. Ex-vivo indention tests were performed on the orbital floor soft tissue of four sheep specimens. The resulting force-displacement data was incorporated into an inverse finite element model to obtain the hyperelastic mechanical properties of the tissue. Material characterization was performed for polynomial, Yeoh, Mooney-Rivlin, and neo-Hookean hyperelastic models using a sequential quadratic programming algorithm. Experimental results indicated relatively large elastic deformation, up to 6 mm, during the indentation test with considerable nonlinearity in the force-displacement response. All hyperelastic models could satisfy the convergence criteria of the optimization procedure, with the highest convergence rate and close fitting accuracy associated with the Yeoh hyperelastic model. The initial guess of the material constants was found to affect the number of iterations before converging, but not the optimization results. The normalized mean square errors of fitting between the model and experimental curves were obtained as 2.39%, 4.26%, and 4.65% for three sheep samples, suggesting that the Yeoh model could adequately describe the typical hyperelastic mechanical behavior of the sino-nasal tissue for surgery simulation.

1. Introduction

Endoscopic Sinus and Skull base Surgery (ESSS) is a minimally invasive technique for the treatment of lesions of the nose and paranasal sinus, the brain defects, or tumors located at the anterior skull base. A rigid fiber optic lens with a working channel passes through the natural pathways of the nose and sinuses to visualize and access the surgery site and permit the excision or biopsy of the lesion using particular instruments. The surgery outcome is obviously advantageous over open surgery due to the reduced swelling, bleeding, and discomfort and, also, a faster recovery [1].

Despite the progressive technological innovations, the ESSS requires many technical skills [2,3]. On the one hand, the anatomy of the sinus and nasal cavity is complex, and there are many vital neurovascular structures in its proximity that are at risk of injury during surgery, e.g., orbital content, carotid arteries, optic nerve, brain, and other intracranial tissues. On the other hand, the restricted vision, the non-intuitive hand-eye coordination, and the use of a single endoscope for both viewing and instrument manipulation in a narrow space with very limited mobility increase

*. *Corresponding author. Tel.: +98 21 66165532; Fax: +98 21 66000021*
E-mail address: farahmand@sharif.edu (F. Farahmand)

doi: 10.24200/sci.2019.50348.1652

the possibility of mistakes in surgery that may lead to severe consequences. It has been reported that neurosurgery ranks as the most liable specialty amongst all the medical subspecialties to malpractice suits in the US, with over 19% facing a claim each year [4].

In order to perform a safe and effective surgery with no complications, the ESSS trainees require special training programs to gain sufficient hand-eye coordination and instrument manipulation skills [5,6]. Currently, the cornerstone of surgical education is learning through observation, which is increasingly challenged by legal and ethical concerns for patient safety, as well as limited efficiency and high costs of operating room time [7,8]. An alternative approach has been the practice of the surgical procedure on animal or cadaver models; this is again restricted by the fact that it needs special lab facilities and cannot be accomplished repetitively due to ethical and economic problems. The emerging field of surgical simulation provides an opportunity to learn and practice neurosurgical procedures in a virtual environment. By replicating the real surgery conditions, surgical simulation systems enable the trainees to practice diverse types of procedures unlimitedly and, even more importantly, experience complicated situations before facing them on real patients [9,10].

The two main components of a surgical simulation system are: (1) An interactive graphical environment of surgery site that is manipulated with virtual surgical tools and (2) A robotic interface, preferably with force feedback capability, which associates the operator's hands with virtual surgical tools. A number of surgical simulation systems have been introduced in recent years for endoscopic sinus surgery training, with a wide range of competencies for each of the above components, particularly the level of force feedback and haptics capability of the robotic interface [11–13]. This is not surprising considering the fact that the sense of touch is an important skill for neurosurgeons to learn and master, in view of a limited degree of finger/hand movements in endoscopic neurosurgery and the presence of vital neurovascular structures in the field [14,15].

Although the implementation of a simple force feedback as a collision detection algorithm is relatively simple, the reconstruction of a realistic sense of haptics in surgical simulation systems is much complicated and challenging. On the one hand, it requires real-time mechanical models of the tissues under surgery to calculate the tool-tissue force interactions and, on the other hand, needs highly efficient control strategies to feedback the forces into the surgeon's hands in real time [16,17]. The tissue models that are currently utilized in neurosurgery simulation systems often contain detailed anatomical descriptions; however, they lack accurate and validated mechanical properties. This limitation restricts the systems' capacity for the reconstruction of a real sense of haptic and, consequently, reduces their overall training efficacy [18].

A review of the related literature shows that the previous attempts for developing tissue mechanical models for surgery simulation have been often devoted to abdominal and thoracic soft tissues [19–21]. There are several reports of the elastic [22–24], hyper elastic [25–27], and viscoelastic [28–30] properties of liver, lung, and breast. The few studies concerning the mechanical properties of tissues involved in neurosurgery simulation are limited to the elastic and viscoelastic properties of the brain [31–33]. To the best of our knowledge, the mechanical behavior of the sino-nasal tissue has not been investigated before.

The aim of this research is to provide a simple, yet realistic, model of the sino-nasal tissue as a major requirement for developing more efficient ESSS simulation systems. Ex-vivo indention tests were performed on the sino-nasal tissue at the posterior of the orbital floor area of sheep specimens, and the force-displacement results were incorporated into an inverse finite element model to obtain the hyperelastic mechanical properties of the tissue by the optimization technique. This paper is organized as follows. In Section 2.1, the specimens, the experimental setup, and the test procedure are introduced. Four candidate hyperelastic models and the finite element model of the indentation test are described in Section 2.2. The inverse finite element modeling and the optimization procedure are presented in Section 2.3. The results of the study are revealed and discussed in Section 3. Finally, Section 4 gives the concluding remakes and future works.

2. Materials and methods

2.1. Experiments

Four heads of adult sheep were acquired from a local abattoir and used as the test samples. Experiments were performed ex-vivo to measure the mechanical properties of the sheep's sino-nasal region as a model of the human one. The sheep's sino-nasal region is frequently used as a benchmark in many endoscopic sinus surgery research works [4], considering its rather similar behavior to the human tissue. The experimental setup and protocol were approved by the ethical committee of the Tehran University of Medical Sciences, Iran.

Prior to the main experiments, a model surgery was performed by an experienced ENT surgeon in order to identify the most appropriate anatomical site within the sino-nasal region of the test samples that provides an intraoperative sense of touch similar to that of the human tissue. The approach used in the model surgery is typically the same as real endoscopic neurosurgery with the exact position of the anatomical site, determined using a surgical navigation system. For one of

the test samples, high-resolution CT images (0.625 mm slice thickness) were acquired, while eight fiducial markers were implanted on the skull for registration (Figure 1(a)). The markers were custom made from ABS to prevent artefacts, yet could be easily recognized in the CT images and by the tracking system [34].

During the model surgery, the surgeon held an endoscope with his left and a curette and the suction with his right hand. While the position of the tip of the instrument was recorded by the surgical navigation system (Figure 1(b)), the surgeon touched and pressed the sinuses and nasal tissue to open the cavities towards the base of the skull. The anatomical sites with an intraoperative sense of touch similar to that of the human were identified and recorded by the surgical navigation system. Figure 2 represents a coronal view of the sino-nasal tissue in the orbital floor area of the sheep sample, which was found most similar to the human tissue and, also, a critical site during ESSS.

In order to measure and characterize the biomechanical properties of the sino-nasal tissue in the selected anatomical site, the main experiments were performed on the three other test samples. An INSTRON test machine (5560 Series Table Model) with 50 kN force capacity and 0.001–500 mm/min speed range was employed to obtain the force-deformation behavior of the orbital floor soft tissue using indentation tests. The accuracy of the load cell was in the range of $+/-0.5\%$ of the indicated force and that of the encoder within $+/-1$ μm.

A custom-made indenter was attached to the moving crosshead of the test machine as the loading probe. The indenter was designed and fabricated in analogy to the curette surgical instrument, as a 4 mm diameter rod with a rounded tip. During the experiments, the test sample was secured to the base of the test machine using two parallel plates, such that the posterior pole of the orbital floor hemisphere was aligned vertically under the indenter. The force-displacement data were acquired at a rate of 1 kHz, while the indenter pressed the sino-nasal tissue at a rate of 10 mm/min. For each sample, a total of six indentation cycles were performed, from which the first five were used for preconditioning to minimize the effect of loading history [35]. The force-displacement data of the last indentation test were used for the analysis.

2.2. Finite element modeling

Considering the large deformation and non-linear mechanical behavior of the sino-nasal soft tissue during the indentation tests, hyperelastic models were used to describe the stress-strain relationship of the tissue in the elastic region. A number of different strain energy functions were proposed to obtain the constitutive equations of hyperelastic materials. This study investigated the compatibility of four popular forms of the strain energy function, e.g., polynomial, Yeoh, Mooney-Rivlin, and neo-Hookean, with the mechanical behavior of the tissue assumed to be isotropic and incompressible. The polynomial strain energy function

(a) (b)

Figure 1. (a) The sheep head specimen with the fiducial markers attached. (b) The surgical navigation system used for tracking the position of the tip of the instrument.

Figure 2. The coronal orbital floor in the sino-nasal region of the sheep found most similar to the human tissue and also a critical site during ESSS.

is defined in the following [36]:

$$U = \sum_{i,j=0}^{\infty} C_{ij}(I_1 - 3)^i (I_2 - 3)^j + \sum_{i=1}^{N} \frac{1}{D_i}(J_{el} - 1)^{2i}, \quad (1)$$

where C_{ij} represents the material hyperelastic constants with the units of force per unit area, I_1 and I_2 are the strain invariants, J_{el} is the elastic volume rate, and D_i is the compressibility coefficient [37]. By employing a second-order polynomial strain energy function in this study, the hyperelastic behavior of the sino-nasal tissue is characterized by five material constants $(C_{10}, C_{01}, C_{20}, C_{11}, C_{02})$ that are determined from the results of the indentation test.

The Yeoh strain energy is a modified version of the $N = 3$ polynomial model, which is only a function of I_1 strain invariant. It has the following form [38]:

$$U = \sum_{i=1}^{3} C_{i0}(I_1 - 3)^i + \sum_{i=1}^{N} \frac{1}{D_i}(J_{el} - 1)^{2i}, \quad (2)$$

where C_{i0} represents the material constants and other parameters are the same as in Eq. (1). Considering the difficulty of measuring the influence of I_2 on the strain energy, this function provides a simpler representation for the strain energy and might improve the ability of the model in predicting the tissue behavior [39].

The Mooney-Rivlin strain energy function is also a special case of the polynomial hyperelastic model with the following form [40]:

$$U = C_{10}(I_1 - 3) + C_{01}(I_2 - 3)^2 + \frac{1}{D_1}(J_{el} - 1)^2, \quad (3)$$

where C_{01}, C_{10}, and D_1 are the material constants, and the other parameters are the same as in Eq. (1). Finally, assuming that $C_{01} \equiv 0$, Eq. (3) is reduced to the strain energy function of the neo-Hookean strain energy model with the following form [41]:

$$U = C_{10}(I_1 - 3) + \frac{1}{D_1}(J_{el} - 1)^2, \quad (4)$$

in which all parameters were defined before.

In order to determine the material constants of the sino-nasal tissue, according to the expressions of Eqs. (1) to (4), a Finite Element Model (FEM) of the tissue under the indentation test was developed and executed in ABAQUS 6.14 [42]. The 3D reconstruction of the orbital floor of the first specimen, obtained from the CT data, is shown in Figure 3.

The geometry of the floor was simplified into a hemisphere (36 mm diameter), with the sinu-nasal tissue at its posterior represented as a homogenous soft tissue with a constant thickness rate of 9 mm. Considering the symmetry of the indenter-tissue interaction,

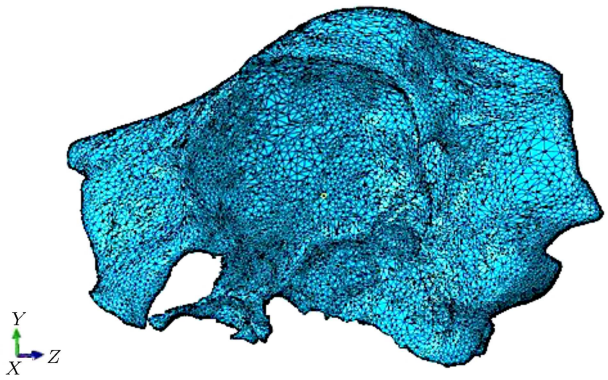

Figure 3. The 3D reconstruction of the orbital floor area of the sheep's head (anterior view).

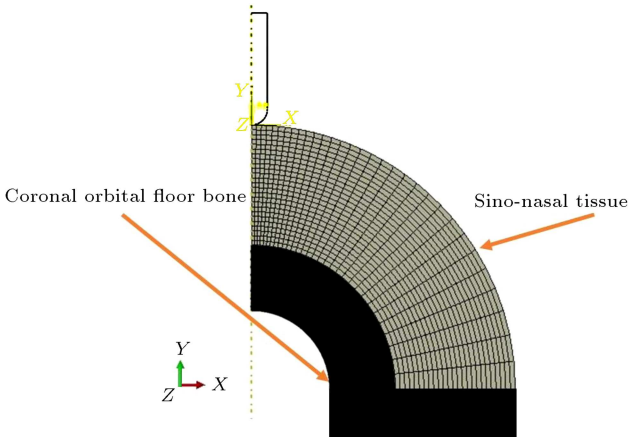

Figure 4. The axisymmetric finite element model of tissue under the indentation test and the introduced boundary conditions.

the FEM was constructed as an axisymmetric model, as shown in Figure 4.

The bony orbital floor was assumed to be rigid, considering its much higher stiffness than that of the sino-nasal soft tissue. Moreover, the indenter was represented by a rigid body with a spherical tip. The sino-nasal tissue was meshed such that it included a finer and higher density mesh close to the contact area with an intender (Figure 4). The element type used for the tissue was an axisymmetric quadrilateral, 4-node bilinear, hourglass control element with reduced integration (CAX4R). After a convergence study with different mesh sizes, a 1083-element model was found to provide results independent of the mesh size.

As the boundary conditions of the model, the symmetry axis was constrained in the horizontal direction, i.e., X axis, and the attachment sites of the tissue and the bony orbital floor in both horizontal and vertical directions, i.e., X and Y, respectively (Figure 4). The indenter was allowed to move only in the Y direction along the symmetry axis, and its motion was imposed on the model by a velocity

boundary condition of 10 mm/min. This velocity boundary condition worked as a simple displacement boundary condition in the analysis of the model using ABAQUS/EXPLICIT solver, considering the fact that the viscoelastic properties of the sino-nasal tissue and the dynamic effects associated with the moving indenter were ignored. The interaction between the indenter tip and the tissue was modeled using contact elements to facilitate simulating their changing contact area for different indentions. The contact between the tip and the tissue was assumed to be frictionless.

2.3. Material characterization

An inverse finite element analysis approach was employed in this study for the hyperelastic material characterization of the sino-nasal tissue. For each of the hyperelastic models, expressed by Eqs. (1) to (4), the material constants changed iteratively to find a finite element solution that best fits with the results of the indentation tests. Figure 5 summarizes the algorithm used for this purpose. For each hyperelastic material constant set, the indentation force data, corresponding with different levels of deformations, were determined from the FEM and compared with those of the experiment. If the deviation of the model and experimental forces were larger than a predefined value, the material constants were changed systemically to obtain a new force data from the model. This procedure was repeated until an acceptable fit was obtained between the model and experimental results, revealing the material constants of the tissue for the chosen hyperelastic model.

In order to change the material constants of the tissue systemically in the iterative finite element analyses and achieve a high optimization convergence trend, Sequential Quadratic Programming (SQP) algorithm [43] was used in this study. This algorithm is available in fmincon (find a minimum of constrained nonlinear multivariable function) solver of MATLAB optimization toolbox (Mathworks, Inc.) [44] and was implemented in ABAQUS using the Python script. The cost function, which should be minimized by the solver, was defined as the Normalized Mean Square Deviation (NMSD) between the FEM forces ($F^{FEM}(C_{ij})$) and the corresponding experimental forces (F^{EXP}):

$$\min_{C_{ij}} NMSD(C_{ij}) = \frac{\sum_{k=1}^{n} \left(F_k{}^{EXP} - F_k{}^{FEM}(C_{ij})\right)^2}{\sum_{k=1}^{n} F_k{}^{\exp 2}}. \quad (5)$$

The C_{ij} in Eq. (5) represents the hyperelastic material constants of the tissue, which are restricted to those variations in a predefined range during the optimizing

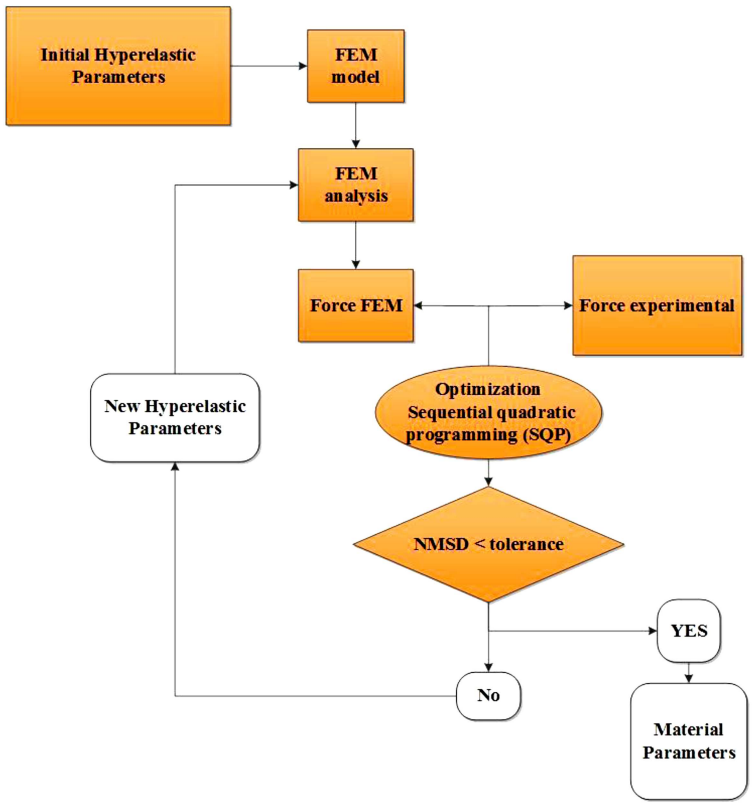

Figure 5. Flowchart of the material characterization algorithm based on the inverse finite element analysis and sequential quadratic programming.

process:

$$L_b \leq C_{ij} \leq u_b, \tag{6}$$

where constants L_b and u_b are the lower and upper bounds, respectively.

As depicted in Figure 5, the algorithm starts by constructing the FEM of the tissue based on an initial guess for material constants. After running the model, the model predictions for indentation forces are determined at different levels of tissue deformation and compared with the corresponding experimental forces, as the reference. Then, by calculating the NMSD, the SQL algorithm updates the material constants to begin a new analysis. This process continues until a predefined acceptable minimum error (tolerance value) condition is satisfied for NMSD, leading to the optimum material constants. The tolerance value was set at 5% in this study.

In order to ensure the reliability of the results of the material characterization approach employed, some further investigations were performed. As indicated in [45], a well-posed mathematical model of a physical phenomenon should have the properties of:

(a) Existence, which means there is a solution for the problem;

(b) Uniqueness, which means there is no more than one solution to the problem;

(c) Stability, which means the solution's behavior is independent of the initial conditions.

The possession of these properties by the material constant results of this study was examined mainly by changing the initial guess of the material constants in their allowable domain (Eq. (6)) and executing the material characterization algorithm repeatedly. It was assumed that the material constant results would be acceptable if the same results were obtained from different initial guesses. This ensures that the optimized material constants determined by the material characterization algorithm are independent of the initial guess, global and unique.

Considering a large number of the finite element analyses required for material characterization using the above approach, it was necessary to make the computational time as short as possible. Before the main analyses, a pilot study was performed to identify the effect of the number of CPUs on the computational time. After running the FEM on PC characterized by a 3.40 GHz Intel (R) Core i7 CPU, and 8 GB of RAM, it was found that the application of five CPU processors would provide the least running time (17 min/run) with no improvement by the larger number of processors.

3. Results and discussion

A typical illustration of the results of the finite element analysis of the sino-nasal tissue subjected to the indentation test is shown in Figure 6. The deformation of the tissue indicated a large deformation just under the indenter tip, which decreased sharply when distancing from the contact site. Similarly, the von Mises stress and contact pressure distributions, shown in Figure 6, indicated large stress and contact pressures in the sino-nasal tissue at the tissue-indenter interface, which disappeared by distancing from the contact zone.

The force-displacement results of the indentation test of one of the sheep sino-nasal tissue samples, as well as the efficacy of the SQL optimization algorithm for material characterization, based on the four hyperelastic models investigated in this study, are shown in Figure 7. The sino-nasal tissue experienced relatively large elastic deformation, up to 6 mm, during the indentation test with considerable nonlinearity in the force-displacement response. This observation supports the use of hyperelastic material

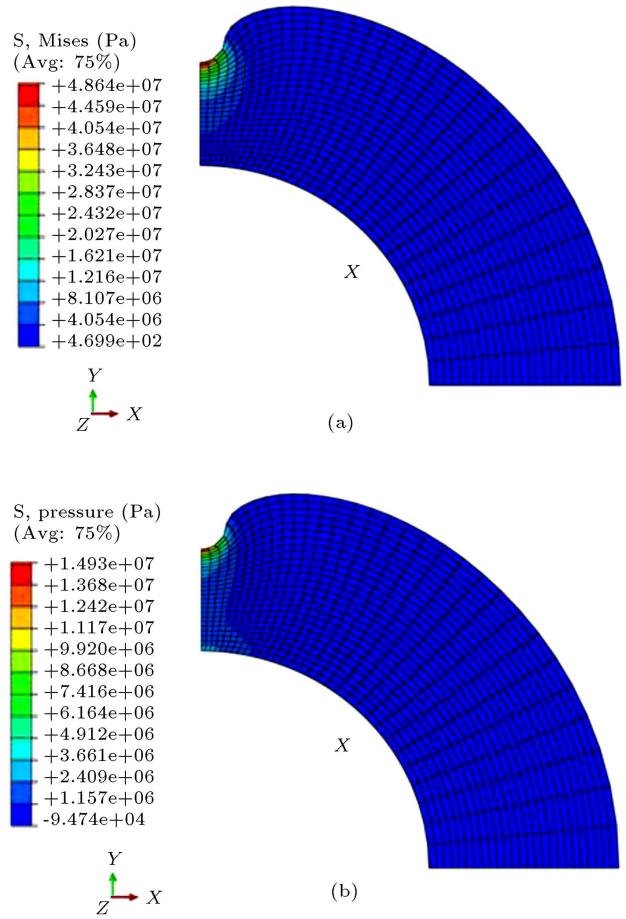

Figure 6. A typical illustration of the results of the finite element analysis of the sino-nasal tissue subjected to the indentation test: (a) The von Mises stress and (b) contact pressure distributions using the iso-stress contours.

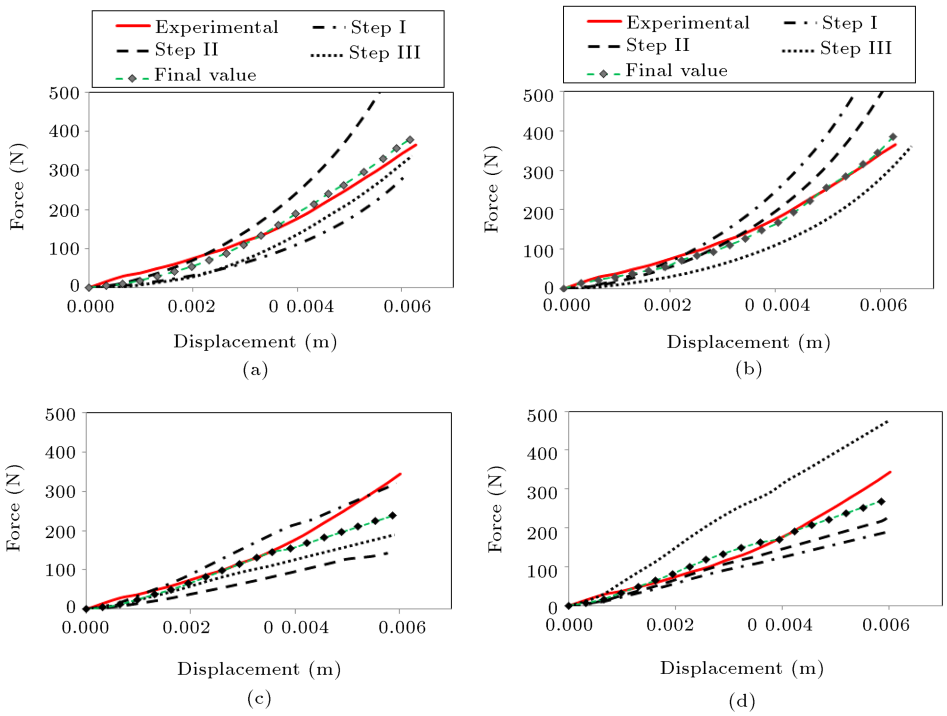

Figure 7. The force-displacement results of the indentation test of one of the sheep sino-nasal tissues, along with the responses of the hyperelastic models at different iterations of the optimization process: (a) Polynomial, (b) Yeoh, (c) Mooney-Rivlin, and (d) neo-Hookean.

models for describing the mechanical behavior of the sino-nasal tissue.

Figure 7 also exhibits how the force-displacement response of the four hyperelastic models based on the initial guesses of the material constants, gradually converges to the experimental results during the SQL optimization process. For all models, the final response, obtained based on the optimized material constants, had a relatively good fit with the experimental data and could satisfy the acceptable maximum fitting error (Eq. (6)).

The number of iterations, however, was different for the four models. In general, the neo-Hookean and the polynomial hyperelastic models revealed the lowest and highest convergence rates, respectively. This is not surprising considering the fact that these two models also have the smallest and largest degrees of freedom, i.e., the number of material constants, respectively. The effect of the initial guess on the number of iterations and the final results of the optimization process are shown in Table 1. The initial guess of the material constants had a considerable effect on the number of iterations required to converge to the optimal condition, particularly for the neo-Hookean and Mooney-Rivlin hyperelastic models. However, regardless of the initial guess, the convergence rate of different hyperelastic models had the same trend, as described before: lowest for neo-Hookean and highest for polynomial hyperelastic models. The final results of the optimization process, i.e., the optimized material constants of each hyperelastic model, however, were not affected by the initial guess, and the same results were obtained for the different initial conditions examined. This observation is very important since it indicates that the optimized material constants determined for each of the hyperelastic models are independent of the initial guess, global and unique.

Table 1 summarizes the NMSD results of the optimized material constants of the first sheep's sino-nasal tissue, obtained for each of the four hyperelastic models. In general, all models could satisfy the convergence criteria, i.e., the 5% tolerance value in Eq. (6), with the NMSDs in the range of 1.64% to 4.96%. The best fitting between the modeling and experimental results was found for the polynomial and, then, for Yeoh hyperelastic model. The neo-Hookean and Mooney-Rivlin models were associated with higher NMSDs due to their relatively poor performance at large displacements (see Figure 7(c) and (d), respectively), which is consistent with the findings of previous studies [41]. Considering the small difference in the NMSD results of the polynomial and Yeoh models, the Yeoh model seems to be more appropriate for the reconstruction of the hyperelastic behavior of the tissue in a surgical simulation system in view of its simple structure and the lower number of parameters.

The results of employing the Yeoh hyperelastic model for the three sheep sino-nasal tissue samples

Table 1. The effect of the initial guess on the number of iterations and the final values of the optimization process. All material constants are in MPa.

Hyperelastic model	Material constant	Step I		Step II		Step III		Final value (MPa)	NMSD
		Initial guess	No of iterations	Initial guess	No of iterations	Initial guess	No of iterations		
Neo-Hookean	C_{10}	1.7	31	2	24	4.5	29	2.2433	0.0496
Mooney-Rivlin	C_{10}	0.5	26	0.7	19	1.2	22	0.9128	0.0356
	C_{01}	0.5		0.7		1.2		0.9046	
Yeoh	C_{10}	0.7	15	1.3	9	1.7	12	1.2512	0.0201
	C_{20}	0.7		1.3		1.7		1.1512	
	C_{30}	0.7		1.3		1.7		0.8921	
Polynomial ($N = 2$)	C_{10}	0.3	12	0.55	11	0.7	14	0.7123	0.0164
	C_{01}	0.3		0.55		0.7		0.4545	
	C_{20}	0.3		0.55		0.7		0.3371	
	C_{11}	0.3		0.55		0.7		0.4242	
	C_{02}	0.3		0.55		0.7		0.2011	

are shown in Figure 8. The force-displacement responses produced by the model are compared with the experimental behavior of the tissues under indentation tests. Considering the naturally expected difference in the material properties of the three tissue samples, their experimental results were dissimilar; consequently, a different set of hyperelastic material constants was obtained for each sample during material characterization (Table 2). However, the reasonably acceptable fitting of the experimental and modeling force-displacement curves indicates that the Yeoh model can adequately describe the hyperelastic mechanical behavior of the sino-nasal tissue. The LSCEs of the curve fittings were 4.26% for sample I, 4.65% for sample II, and 2.39% for sample III.

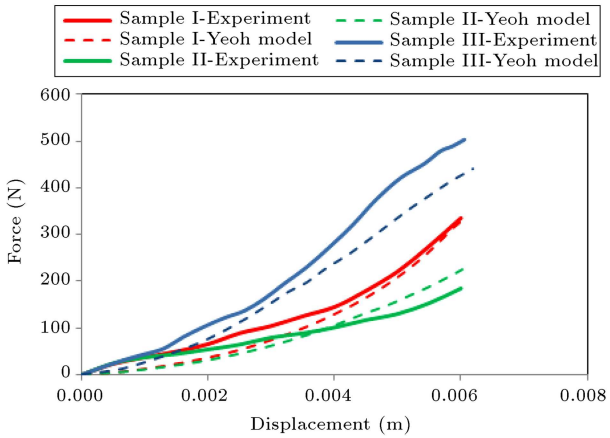

Figure 8. The force-displacement results of the indentation test of the three sheep sino-nasal tissue samples along with the responses of the corresponding Yeoh hyperelastic models.

Table 2. The hyperelastic material constants of the three sheep sino-nasal tissue samples based on the Yeoh strain energy function.

Material constant	Sample I	Sample II	Sample III	Average
C_{10}	0.7541	0.7246	1.7584	1.0791
C_{20}	1.0215	0.4123	1.3553	0.9297
C_{30}	0.9107	0.8568	2.3666	1.5004

The hyperelastic material constants, shown in Table 2, provide the required information to build a simple, yet realistic, mechanical model of the sino-nasal tissue for ESSS simulation systems. The average material constants of the different test samples might seem more practical for the simulation system in order to reconstruct a typical intraoperative sense of touch of endoscopic neurosurgery. However, by using the data of each sample independently, the potential variation of the sense of touch among different specimens, which is observed during real surgery, could be also simulated.

4. Conclusion

The sense of touch is an important skill for endoscopic neurosurgeons to learn and master in view of the limited degree of finger/hand movements during surgery and the presence of vital neurovascular structures in the field. In this study, for the first time, the mechanical properties of the sino-nasal tissue were measured and characterized to provide the required information for the reconstruction of a typical sense of

touch in endoscopic neurosurgery simulation systems. Ex-vivo indention tests were performed on the sino-nasal tissue samples of four sheep specimens, and the force-displacement results were incorporated into an inverse finite element model to characterize a number of hyperelastic material models, i.e., polynomial, Yeoh, Mooney-Rivlin, and neo-Hookean, using optimization technique. The tissue's intrinsically nonlinear mechanical behavior, observed in the experiments, could be described by the hyperelastic models with reasonably good accuracy. In particular, the initial guess of the material constants did not affect the optimization results, suggesting the optimized material constants to be independent, global and unique. Among the hyperelastic models examined, the Yeoh model provided the highest convergence rate with close fitting accuracy with the experimental data, kept preserved for different tissue samples (NMSDs in the range of 2.29% and 4.65%). It was concluded that the Yeoh model provided a simple, yet realistic, representation of the hyperelastic mechanical behavior of the sino-nasal tissue for application in endoscopic neurosurgery simulation systems. The Yeoh material constants of multiple samples provided by this study might be averaged to reconstruct a typical sense of touch or used individually to mimic the variation among different specimens. The results of this study, however, are based on a limited number of sheep samples instead of a human. For a more accurate haptics reconstruction, the tissue model should be based on a larger experimental dataset and particular human specimens. Our preliminary model surgery enabled identifying the most appropriate site within the sino-nasal region of the sheep that provides an intraoperative sense of touch similar to that of the human tissue based on the experience of a skilled neurosurgeon. In spite of this effort, there are minor differences in the mechanical properties of human and sheep sino-nasal tissue that calls for future studies on cadaveric human subjects. Moreover, for the higher efficacy of the surgical simulator, the tissue model should also account for the effects associated with the speed of tissue manipulation by the surgeon, i.e., the strain rate. The development of such a hyper-viscoelastic model of the sino-nasal tissue would need a more comprehensive set of experimental tests on human cadaveric subjects to be performed in the future.

Acknowledgment

The experimental efforts of this study were facilitated by the Djavad Mowafaghian Research Center of Intelligent NeoruRehabilitation Technologies, the Research Center of Biomedical Technology and Robotics at the Research Institute of Medical Technology of Tehran University of Medical Sciences, Amrikabir University of Technology (Tehran Polytechnic). The help of Ehsan Abdollahi in preparing the specimens and experimental setup is also appreciated. This study was supported by a research grant (No: 94-S-44756) from Iran National Science Foundation.

References

1. Al-Mujaini, A., Wali, U., and Alkhabori, M. "Functional endoscopic sinus surgery: indications and complications in the ophthalmic field", *Oman Medical Journal*, **24**(2), pp. 70–80 (2009).
2. Wurm, J., Dannenmann, T., Bohr, C., Iro, H., and Bumm, K. "Increased safety in robotic paranasal sinus and skull base surgery with redundant navigation and automated registration", *The International Journal of Medical Robotics and Computer Assisted Surgery*, **1**(3), pp. 42–48 (2005).
3. Varshney, R., Frenkiel, S., Nguyen, L.H., Young, M., Del Maestro, R., Zeitouni, A., Saad, E., Funnell, W.R.J., and Tewfik, M.A. "The McGill simulator for endoscopic sinus surgery (MSESS): a validation study", *Journal of Otolaryngology-Head & Neck Surgery*, **43**(1), p. 40 (2014).
4. Delgado-Vargas, B., Romero-Salazar, A.L., Burneo, P.M.R., Hincapie, C.V., de los Santos Granado, G., del Castillo López, R., Arnau, C.F., and Marco, I.C. "Evaluation of resident's training for endoscopic sinus surgery using a sheep's head", *European Archives of Oto-Rhino-Laryngology*, **273**(8), pp. 2085–2089 (2016).
5. Kühnapfel, U., Cakmak, H.K., and Maa, H. "Endoscopic surgery training using virtual reality and deformable tissue simulation", *Computers & Graphics*, **24**(5), pp. 671–682 (2000).
6. Parikh, S.S., Chan, S., Agrawal, S.K., Hwang, P.H., Salisbury, C.M., Rafii, B.Y., Varma, G., Salisbury, K.J., and Blevins, N.H. "Integration of patient-specific paranasal sinus computed tomographic data into a virtual surgical environment", *American Journal of Rhinology & Allergy*, **23**(4), pp. 442–447 (2009).
7. Acar, B., Gunbey, E., Bababemez, M.A., Karabulut, H., Gunbey, H.P., and Karasen, R.M. "Utilization and dissection for endoscopic sinus surgery training in the residency program", *Journal of Craniofacial Surgery*, **21**(6), pp. 1715–1718 (2010).
8. Delorme, S., Laroche, D., DiRaddo, R., and Del Maestro, R.F. "NeuroTouch: a physics-based virtual simulator for cranial microneurosurgery training", *Operative Neurosurgery*, **71**(1 Suppl Operative), pp. 32–42 (2012).
9. Zhao, Y.C., Kennedy, G., Yukawa, K., Pyman, B., and O'Leary, S. "Can virtual reality simulator be used as a training aid to improve cadaver temporal bone dissection? Results of a randomized blinded control trial", *The Laryngoscope*, **121**(4), pp. 831–837 (2011).
10. Kolbari, H., Sadeghnejad, S., Bahrami, M., and Ali, K.E. "Adaptive control of a robot-assisted tele-surgery

in interaction with hybrid tissues", *Journal of Dynamic Systems, Measurement, and Control*, **140**(12), p. 121012 (2018).

11. Wiet, G.J., Stredney, D., and Wan, D. "Training and simulation in otolaryngology", *Otolaryngologic Clinics of North America*, **44**(6), pp. 1333–1350 (2011).
12. Kolbari, H., Sadeghnejad, S., Bahrami, M., and Kamali, A. "Bilateral adaptive control of a teleoperation system based on the hunt-crossley dynamic model", In: *Robotics and Mechatronics (ICROM), 3rd RSI International Conference on 2015*, pp. 651–656, IEEE (2015).
13. Kolbari, H., Sadeghnejad, S., Bahrami, M., and Kamali, E.A. "Nonlinear adaptive control for teleoperation systems transitioning between soft and hard tissues", In: *Robotics and Mechatronics (ICROM), 2015 3rd RSI International Conference on*, pp. 055–060, IEEE (2015).
14. Piromchai, P. "Virtual reality surgical training in ear, nose and throat surgery", *International Journal of Clinical Medicine*, **5**, pp. 558–566 (2014).
15. Rosseau, G., Bailes, J., del Maestro, R., Cabral, A., Choudhury, N., Comas, O., Debergue, P., De Luca, G., Hovdebo, J., and Jiang, D. "The development of a virtual simulator for training neurosurgeons to perform and perfect endoscopic endonasal transsphenoidal surgery" *Neurosurgery*, **73**, pp. S85–S93 (2013).
16. Samur, E., Sedef, M., Basdogan, C., Avtan, L., and Duzgun, O. "A robotic indenter for minimally invasive measurement and characterization of soft tissue response", *Medical Image Analysis*, **11**(4), pp. 361–373 (2007).
17. Sadeghnejad, S., Esfandiari, M., Farahmand, F., and Vossoughi, G. "Phenomenological contact model characterization and haptic simulation of an endoscopic sinus and skull base surgery virtual system", In *Robotics and Mechatronics (ICROM), 4th International Conference on*, pp. 84–89, IEEE (2016).
18. Ebrahimi, A., Sadeghnejad, S., Vossoughi, G., Moradi, H., and Farahmand, F. "Nonlinear adaptive impedance control of virtual tool-tissue interaction for use in endoscopic sinus surgery simulation system", In: *Robotics and Mechatronics (ICROM)*, 4th International Conference on 2016, pp. 66–71, IEEE (2016).
19. Fu, Y. and Chui, C. "Modelling and simulation of porcine liver tissue indentation using finite element method and uniaxial stress–strain data", *Journal of Biomechanics*, **47**(10), pp. 2430–2435 (2014).
20. Cheng, L. and Hannaford, B. "Evaluation of liver tissue damage and grasp stability using finite element analysis", *Computer Methods in Biomechanics and Biomedical Engineering*, **19**(1), pp. 31–40 (2016).
21. Dehghani Ashkezari, H., Mirbagheri, A., Behzadipour, S., and Farahmand, F. "A mass-spring-damper model for real time simulation of the frictional grasping interactions between surgical tools and large organs", *Scientia Iranica*, **22**(5), pp. 1833–1841 (2015).
22. Zeng, Y., Yager, D., and Fung, Y. "Measurement of the mechanical properties of the human lung tissue", *Journal of Biomechanical Engineering*, **109**(2), pp. 169–174 (1987).
23. Al-Mayah, A., Moseley, J., and Brock, K. "Contact surface and material nonlinearity modeling of human lungs", *Physics in Medicine & Biology*, **53**, p. 305 (2007).
24. Saghaei Nooshabadi, Z., Abdi, E., Farahmand, F., Narimani, R., and Chizari, M. "A meshless method to simulate the interactions between a large soft tissue and a surgical grasper", *Scientia Iranica*, **23**(1), pp. 295–300 (2016).
25. Mehrabian, H., Campbell, G., and Samani, A. "A constrained reconstruction technique of hyperelasticity parameters for breast cancer assessment", *Physics in Medicine and Biology*, **55**(24), p. 7489 (2010).
26. Naini, A.S., Patel, R.V., and Samani, A. "Measurement of lung hyperelastic properties using inverse finite element approach. Biomedical Engineering", *IEEE Transactions on*, **58**(10), pp. 2852–2859 (2011).
27. Cheng, L. and Hannaford, B. "Finite element analysis for evaluating liver tissue damage due to mechanical compression", *Journal of Biomechanics*, **48**(6), pp. 948–955 (2015).
28. Kobayashi, Y., Kato, A., Watanabe, H., Hoshi, T., Kawamura, K., and Fujie, M.G. "Modeling of viscoelastic and nonlinear material properties of liver tissue using fractional calculations", *Journal of Biomechanical Science and Engineering*, **7**(2) pp. 177–187 (2012).
29. Fallah, A., Ahmadian, M.T., and Aghdam, M.M. "Rate-dependent behavior of connective tissue through a micromechanics-based hyper viscoelastic model", *International Journal of Engineering Science*, **121**, pp. 91–107 (2017).
30. Panda, S.K. and Buist, M.L. "A finite nonlinear hyper-viscoelastic model for soft biological tissues", *Journal of Biomechanics*, **69**, pp. 121–128 (2018).
31. Karimi, A., Navidbakhsh, M., Haghi, A.M., and Faghihi, S. "Measurement of the uniaxial mechanical properties of rat brains infected by plasmodium berghei ANKA", *Proceedings of the Institution of Mechanical Engineers, Part H: Journal of Engineering in Medicine*, **227**(5), pp. 609–614 (2013).
32. Karimi, A., Navidbakhsh, M., Yousefi, H., Haghi, A.M., and Sadati, S.A. "Experimental and numerical study on the mechanical behavior of rat brain tissue", *Perfusion*, **29**(4), pp. 307-314 (2014).
33. Rashid, B., Destrade, M., and Gilchrist, M.D. "Mechanical characterization of brain tissue in simple shear at dynamic strain rates", *Journal of the Mechanical Behavior of Biomedical Materials*, **28**, pp. 71–85 (2013).
34. Trévillot, V., Sobral, R., Dombre, E., Poignet, P., Herman, B., and Crampette, L. "Innovative endoscopic sino-nasal and anterior skull base robotics",

International Journal of Computer Assisted Radiology and Surgery, **8**(6), pp. 977–987 (2013).

35. Martin, C., Pham, T., and Sun, W. "Significant differences in the material properties between aged human and porcine aortic tissues", *European Journal of Cardio-Thoracic Surgery*, **40**(1), pp. 28–34 (2011).
36. Rivlin, R.S. and Saunders, D. "Large elastic deformations of isotropic materials. VII. Experiments on the deformation of rubber", *Philosophical Transactions of the Royal Society of London A: Mathematical, Physical and Engineering Sciences*, **243**(865), pp. 251–288 (1951).
37. Kaster, T., Sack, I., and Samani, A. "Measurement of the hyperelastic properties of ex vivo brain tissue slices", *Journal of Biomechanics*, **44**(6), pp. 1158–1163 (2011).
38. Yeoh, O. "Characterization of elastic properties of carbon-black-filled rubber vulcanizates", *Rubber Chemistry and Technology*, **63**(5), pp. 792–805 (1990).
39. Mehrabian, H. and Samani, A. "An iterative hyperelastic parameters reconstruction for breast cancer assessment" In: *Medical Imaging*, **6916**, 69161C. International Society for Optics and Photonics (2008).
40. Mooney, M. "A theory of large elastic deformation", *Journal of Applied Physics*, **11**(9) pp. 582–592 (1940).
41. Ogden, R.W., *Non-linear Elastic Deformations*, Courier Corporation (1997).
42. Manual, A.U., Version 6.14–1, Dassault Systémes Simulia Corp., Providence, RI.
43. Schittkowski, K. "NLPQL: A FORTRAN subroutine solving constrained nonlinear programming problems", *Annals of Operations Research*, **5**(2), pp. 485–500 (1986).
44. Guide, M.U.s., The mathworks, Inc., Natick, MA **5** p. 333 (1998).
45. Hadamard, J., *Lectures on Cauchy's Problem in Linear Partial Differential Equations*, Courier Corporation, (2014).

Biographies

Soroush Sadeghnejad received his BSc and MSc in Mechanical Engineering from Amirkabir University of Technology with top ranks in 2009 and 2011. Since then, he has been a PhD student at Sharif University of Technology. He is also currently a Research Associate and a Lecturer at the Mechanical Engineering Department of Amirkabir University of Technology. His research is focused on the medical and surgery robotics, haptic, and control, especially on the field of mobile robots, human-like robots, robotics systems, and automation. He has published several papers in journals, conferences, and symposiums. He is a member of IEEE Robotics and Automation society and the Robotics society of Iran.

Nahid Elyasi received her MSc in Materials Science and Engineering, majoring in metal forming, from the Materials Engineering Department of Sharif University of Technology in 2014. She is presently an MSc Student at the University of Alberta. Her research interests include nonlinear elasticity, FEM, and biomechanics.

Farzam Farahmand received his PhD in Mechanical Engineering-Biomechanics, from Imperial College of Science, Technology and Medicine, London, UK in 1996. He is currently a Professor and the Head of the Biomechanics Division at the Mechanical Engineering Department of Sharif University of Technology, Tehran, Iran. He also has a joint appointment in the Research Center for Biomedical Technologies and Robotics (RCBTR) at Tehran University of Medical Sciences, Tehran, Iran, where he is the Head of the Medical Robotics Group. His research is focused on human motion, orthopedic biomechanics, and medical robotics. In his career, he has developed several medical instruments and devices and published numerous journal and conference papers in different fields of biomechanics and biomedical robotics.

Gholamreza Vossoughi received his PhD from Mechanical Engineering Department at University of Minnesota in 1992. Ever since, he has been a faculty member of Mechanical Engineering at Sharif University of Technology. He has served as the Manufacturing Engineering and Applied Mechanics Division Directors from 1994-1998 and as the Graduate Dean of the Mechanical Engineering Department from 1999-2003 and the Dean of the Mechanical Engineering Department from 2012-2014. He has also served as the founder/director of the Mechatronics Engineering program at both Sharif's main campus and Sharif's international campus at Kish Island from 2004. His research interests include bio-inspired robotics, man-machine interface and haptic systems, mechatronics, and control systems.

Seyed Mousa Sadr Hosseini has been an Associate Professor of Otolaryngology at the Tehran University of Medical Sciences since 1996. His research interests include the emerging trends in sinus surgery, functional endoscopic sinus surgery, and diseases of the nose and sinuses on which he published several scientific papers in national and international conferences and journals. He is a member of Iranian Otolaryngologic Society, Board of Yearly Otolaryngology Residency Examination, Council of Graduate Medical Education, and Board of Residency Entry Examination.